International Journal of Research Studies on Environment, Earth, and Allied Sciences (IJRSEAS)
| Volume-2 Issue-4 |August-2025 | ISSN: 3066-0637 | Website: https://eesrd.us

Manuscript ID:
IJRSEAS-2025-020402

OPEN ACCESS

Quick Response Code:

Website: https://eesrd.us

DOI: 10.5281/zenodo.17090234

DOI Link:
https://doi.org/10.5281/zenodo.17090234

Volume: 2

Issue: 4

Pp. 4-9

Month: August

Year: 2025

E-ISSN: 3066-0637

Submitted: 06 July 2025

Revised: 10 July 2025

Accepted: 10 Aug 2025

Published: 31 Aug 2025

Address for correspondence:
Sunil Kawade
Bhasker Pandurang Hiwale Education Society's Ahmednagar College, Ahmednagar SPPU India
Email: kawades756@gmail.com

How to cite this article:
Kawade, S., Bobade, D. H., & Kawade, A. (2025). Structural, Optical and Photocatalytic Study of Cobalt doped Zinc Ferrite. International Journal of Research Studies on Environment, Earth, and Allied Sciences, 2(4), 4–9. https://doi.org/10.5281/zenodo.17090234

Structural, Optical and Photocatalytic Study of Cobalt doped Zinc Ferrite

Sunil Kawade[1], Dr. D. H. Bobade[2], Anil Kawade[3]
[1]Bhasker Pandurang Hiwale Education Society's Ahmednagar College, Ahmednagar SPPU India
[2]Chandmal Tarachand Bora Arts, Commerce & Science College, Shirur, Pune, SPPU India
[3]Research & Development, Arti Industries, Mumbai, India

Abstract

The polycrystalline powder of $Zn_{1-x}Co_xFe_2O_4$ with a variable Co concentration ranging from 0.0 to 0.3 was created using the Sol Gel assisted auto combustion process. The powder X-ray diffraction technique was used to investigate the sample's structural phase identification. The synthesized ferrite material cubic structure with Fd3m space group was shown by X-Ray Diffraction data. The unit cell volume and lattice parameter values have changed slightly as a result of the doping of Co ions, but the crystal structure remains unchanged. In the X- Ray Diffraction data, no additional peaks are observed. In Diffuse reflectance spectroscopy (DRS) shows The band gap of $Zn_{1-x}Co_xFe_2O_4$($x = 0.0 - x = 0.3$) are found to be 3.10ev, 3.07ev, 2.98ev, and 2.92ev Respectively. As Co concentration increases band gap goes on decreasing. Band gap decreases (x=0.0 to x=0.3) that leads to increasing the photocatalytic performance. In photocatalytic degradation as Co concentration increases percentage of degradation increases. The % of Degradation ~ 45% at x= 0.0 as Co concentration increases % of degradation also increases up to the ~73% at x = 0.3 Respectively. The work demonstrates the potential of co-doped zinc ferrite as a powerful photocatalyst driven by visible light.

Keywords: *Zinc ferrite; Spinel Ferrite Co-doping, XRD, UV-DRS, Band Gap, Photocatalysis, Methylene Blue, Nanomaterial*

Introduction

Ferrites are a kind of ferromagnetic materials. [1] ferrites are gaining a lot of attention in scientific research because of their distinct electrical and magnetic properties. There are various application of ferrites such as high-frequency electronics, biomedical fields, wastewater treatment, magnetic storage devices, sensors, and photocatalysis. Researchers are becoming more interested in magnetic nanoparticles because of their unique magnetic and electrical properties. [2-3] The spinel ferrites group of ferrites are grown in various fields. The typical formula for spinel is MFe_2O_4, where M is an ion of a divalent metal. The properties of spinel ferrite changed by doping and the distribution of cations inside the molecule. The cubic crystal structure of spinel ferrites is closed-packed arrangement of metal cations and oxygen ions scattered at tetrahedral (A) and octahedral [B] sites. [4–5]. The chemical mixture of cation distribution at the (A) and [B] sites are the primary determinants of spinel ferrites [6]. Zinc ferrite have various characteristics, such as surface area, surface shape, crystallite size, defect level, optical properties, saturation magnetization, etc., and these characteristics can be tailored further improve structural, magnetic, and catalytic performance by dopants such as cobalt (Co) [7-8]. In Catalysis and wastewater treatment, spinel ferrites are frequently used as magnetic adsorbents and their primary benefit is the ease with which they can be separated from aqueous solutions by applying an external magnetic field [9]. The synthesis method shows a crucial role in investigating the physicochemical properties of $ZnFe_2O_4$ nanoparticles. The desired particle characteristics have been achieved using a variety of techniques, including co-precipitation, hydrothermal synthesis, ball milling, sol-gel, and solid-state methods. Sol-gel auto combustion produces the most uniform and pure nanoparticles at the lowest temperature, since it produces nanoparticles of uniform size with regular microstructures. [10-16]. A sol-gel process creates a network by colloidally suspending solid particles in a liquid to create a sol, which is then gelled into a three-dimensional structure. A rapid exothermic reaction occurs between precursor solution of metal salts and chelating agent (suitable fuels) in sol-gel assisted auto combustion, leading to the formation of the desired material. The gel is formed after the solvent evaporates and remaining particles begin to form interconnected networks after the solvent evaporates and Converting monomers into colloidal solution is called gel formation, that is, it is the formation of colloidal solutions. The end result of the process is colloidal powder films this process guarantees that the final product has a controlled microstructure and a consistent nanoscale dimension.

Furthermore, the low temperature employed makes the approach effective for synthesizing nanoparticles [17-18].as used the sol-gel auto combustion approach to synthesize cobalt-doped zinc ferrite nanoparticles with $C_6H_8O_7 \cdot 2H_2O$ as a chelating agent. The synthesis method has several benefits, such as simplicity, scalability, and the ability to create nanomaterials with specific properties. Because of their various properties, the materials that are produced has variety of application such as energy storage, sensors, biomedical devices, and catalysis [21].in the present study, Sol-Gel auto combustion process was used to prepare $Zn_{1-x}Co_xFe_2O_4$ (x = 0.0, 0.1, 0.2, and 0.3). This approach was chosen due to its low cost, low temperature and easy to handle and straightforward procedure.

Material and Methodology

1. Preparation of $Co_xZn_{1-x}Fe_2O_4$

The starting materials were Zinc Nitrate $Zn(NO_3)_2 \cdot 6H_2O$, Cobalt Nitrate $Co(NO_3)_2 \cdot 6H_2O$, Ferric Nitrate $Fe(NO_3)_2 \cdot 9H_2O$ and citric acid $(C_6H_8O_7) \cdot 2H_2O$ The stoichiometric ratio of metal nitrates to citric acid is 1:1 maintained. The precursors were added in 50 ml distilled water and the solution were stirred in order to attain the homogeneous solution. Then the ammonia was mixed slowly maintaining the pH value equal to 7-8. After that the mixture was continuously stirred at 80 °C – 90 °C for 3 hours. The solution turned into gel when it was heated further. The resultant gel laterally expands into a fluffy mass resembling foam and then undergoes self-propagating combustion and turned to fine powder. The obtained powder was ground for 60 minutes and then it was annealed in a muffle furnace for four hours at 800 °C.

Result and Discussion

2. X- Ray Diffraction

According to the Normalised XRD Pattern, the lattice planes (220), (311), (222), (400), (422), (511) and (440) were present at different 2θ values. The XRD pattern was used to determine the synthesized ferrite nanoparticle's single-phase cubic spinel structure. Strong reflection observed in (311) plane it indicate the spinel phase which belongs to the Fd3m space group [24]. Particles with a broad XRD line indicate that they are nano sized. using Scherrer's equation, the average crystallite size of the samples was calculated. the average crystallite sizes varied between 35 and 45 nm. There was a match between the observed diffraction peaks and JCPDS card number #2210-12 based on their intensity peaks and their d values. Fig. 1 shows the XRD pattern for Co-Zn ferrite. The intense peak (311) is used to calculate the lattice parameter of the spinel ferrite. Zinc ferrite is enriched with Co, the lattice parameter of

$Zn_{1-x}Co_xFe_2O_3$ is reduced to 0.8418 nm, 0.8387 nm, 0.8382 nm, and 0.8304 nm, which is due to the smaller ionic radius of Co^{2+} (0.072 nm) than Zn^{2+} (0.074 nm). Table.1 shows the parameters calculated for the synthesized ferrite using the following equations.

Scherrer's equation accounts for peak broadening due to crystallite size (D). However, peak broadening also results from microstrain (ε) in the crystal lattice. The modified Scherrer equation, which includes both contributions, is given by [26],

$$ln(\beta) = ln(\frac{k\lambda}{D}) + ln(1/cos\theta)$$

Crystallite size is calculated by taking into account lattice strain contribution to peak broadening. Since the peak broadening is caused by micro-strain and crystal size, β_{hkl} expressed as follows:

$$\beta_{hkl} = \beta_{size} + \beta_{strain} \text{ ------(2)}$$

$$\text{But strain is } 4 \cdot \varepsilon \cdot tan\theta \text{ and size is } \frac{k\lambda}{Dcos\theta}$$

$$\therefore \beta_{hkl} = \frac{k \cdot \lambda}{D \cdot cos\theta} + 4 \cdot \varepsilon \cdot tan\theta \text{ ------(3)}$$

$$\therefore \beta_{hkl} \cdot cos\theta = \frac{k \cdot \lambda}{D} + 4 \cdot \varepsilon \cdot sin\theta \text{ ------(4)}$$

The micro strain in the sample is calculated using the formula □/4×tan□ [25-26].

X-ray density of material is given by the following formula,

$$\rho_x = \frac{8M}{Na^3} \text{ -------- (5)}$$

where, M is molecular mass of the sample, N is Avogadro number and 'a' is the lattice parameter. By using sauter's formula to calculate the specific surface area of samples and this specific surface area is important for the heterogeneous catalysis, adsorption and surface reactions.

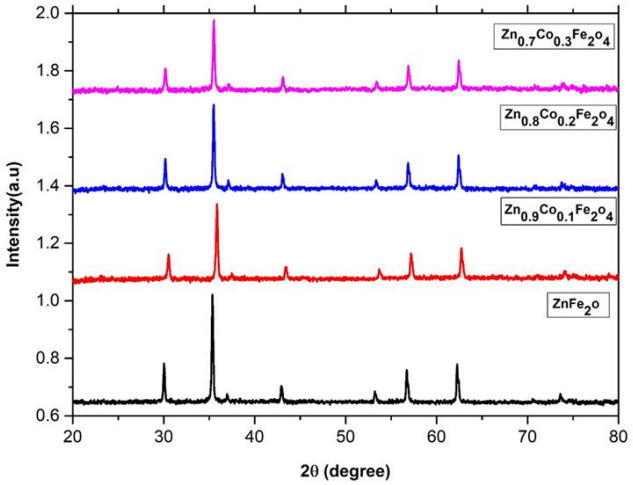

Fig. 1 *XRD Plot $Zn_{1-x}Co_xFe_2O_4$ (x = 0.0, 0.1, 0.2, 0.3)*

Table 1: Structural parameters of $Zn_{1-x}Co_xFe_2O_4$ (x = 0.0, 0.1, 0.2, 0.3) as obtained from X –Ray diffraction Analysis.

Parameters	Co Concentration			
	0.0	**0.1**	**0.2**	**0.3**
V_{cell} $(A^0)^3$	594.31	570.85	587.86	586.96
Crystalline Size(D) (nm) Scherer's equation	0.7449	0.7204	0.6974	0.7211
Lattice Parameter (nm)	0.8418	0.8387	0.8382	0.8304
Interplanary Spacing	2.5353	2.5012	2.5258	2.5245
X-ray Density(ρ_x) $\times 10^{-23}$	189.92	192.36	190.64	190.71
Specific Surface Area (SSA)	69.69	79.70	76.39	83.89
Microstrain $\times 10^{-23}$ (W-H plot)	2.73	2.96	2.58	3.13
Dislocation Density (δ) $\times 10^{-4}$ (Nm^{-2})	4.866	6.527	5.891	7.111

3. UV Visible Diffuse Reflectance spectroscopy(UV-DRS)

UV-Visible diffuse reflectance spectroscopy was used to examine the optical characteristics of un-doped, doped, co-doped nanoparticles. . Fig.2 Shows all the samples show a large dip in the reflectance between 300 nm and 650 nm. In Fig 2. also observed that the absorption edge shift lower wavelength for the concentration of x= 0.0 to higher wavelength x =0.3 concentration. The band gap value is influenced by various factors such as crystallite size, structural parameter, carrier concentrations, presence of impurities and lattice strain[ ]. The diffuse reflectance (R) data is used for the determination of band gap energy by the Kubelka Munk function.

$$F(R) = \frac{(1-R)^2}{2R} \quad ------(1)$$

where, R-reflectance, F(R)-Kubelka-Munk function, A graph is plotted between [F(R).hυ] ^{2} and hυ, The band gap of $Zn_{1-x}Co_xFe_2O_4$ (x = 0.0 to x= 0.3) are found to be 3.10ev, 3.07ev, 2.98ev, and 2.92ev Respectively. The observed band gap narrowing enhances visible-light absorption, making Co-doped $ZnFe_2O_4$ nanoparticles promising candidates for applications in photocatalysis. As the un-doped and doped Co goes from (x=0.0 to x=0.3) band gap goes on decreasing. it could be due to additional energy level which is produced due to doping.

The modified Tauc function

$$F(R)h\upsilon = A(h\upsilon - Eg)^n \quad ---------- (2)$$

where n = 2 and 1/2 represent direct and indirect transitions that give direct and indirect band gap, respectively. In general, Kubelka–Munk (KM) function F(R) given in the Equations (1) and (2) is applied to the diffuse reflectance spectra to obtain the optical band gap. [21-24]

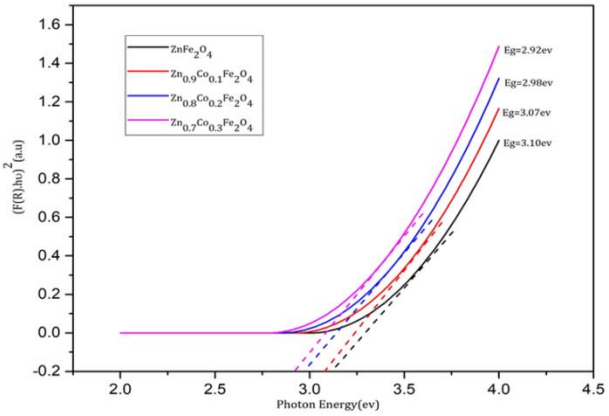

Figure.2 *Tauc plots $(F(R).hv)^2$ vs. photon energy(hv) for $Zn_{1-x}Co_xFe_2O_4$ (x = 0.0, 0.1, 0.2, 0.3) nanoparticles. The linear extrapolation of the plots indicates progressive decrease in optical band gap energy from 3.10 eV (x = 0.0) to 2.92 eV (x = 0.3).*

4. Photocatalytic Degradation.

Using the sol-gel auto-combustion method, zinc ferrite nanoparticles doped with cobalt have been synthesized and evaluated for their photocatalytic activity. Photocatalytic performance was assessed using the degradation of methylene blue dye under visible light. Using methylene blue solution dispersed in 0.15mg of the catalyst in 100 mL, the degradation percentage of the catalyst was monitored over a 60-minute period in each sample (10 min difference), in 100 mL Methylene Blue solution 0.15mg of the catalyst was dispersed. and the degradation percentage was taking up to a 60-minute period. Observed the un - doped $ZnFe_2O_4$ (x = 0.0) exhibited the lowest photocatalytic efficiency, reaching approximately ~ 45% degradation. As the doping of cobalt increases a significant enhancement in degradation efficiency was observed.

$Zn_{0.9}Co_{0.1}Fe_2O_4$ showed ~ 61% degradation, $Co_{0.2}Zn_{0.8}Fe_2O_4$ achieved ~ 67%, and $Co_{0.3}Zn_{0.7}Fe_2O_4$ reached a maximum of ~ 73% degradation within the same duration of time(fig.3). As per the improvement in photocatalytic performance show that the better visible light absorption, efficient charge separation, and reduced electron-hole recombination due to the incorporation of Co^{2+} ions into the Zinc ferrite structure. $Zn_{1-x}Co_xFe_2O_4$ photocatalysts under visible light respectively [25 -30]

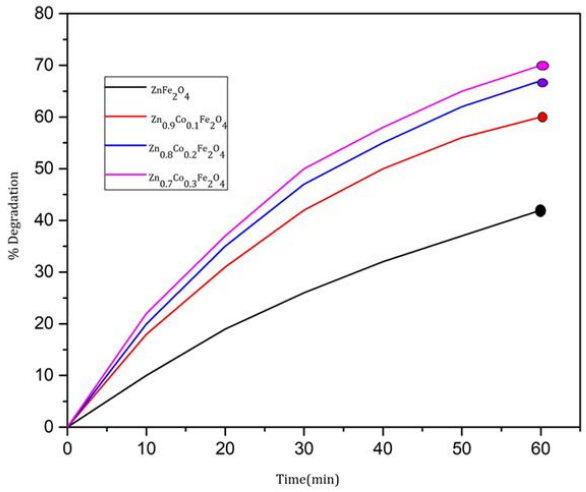

Figure.3 *Time-dependent photocatalytic degradation of methylene Blue dye under visible light irradiation using $Zn_{1-x}Co_xFe_2O_4$(x=0.0, 0.1, 0.2, 0.3)*

Conclusion:

Sol –Gel auto combustion method is successfully applied to synthesize micro particles of cobalt-doped zinc ferrite. According to this XRD plot, cobalt ions were incorporated and zinc ferrite formed. Synthesized ferrite exhibited cubic structure with space group Fd3m. According to UV Diffuse Reflectance Spectroscopy as the doping of cobalt ion increases (x= 0.0 to x= 0.3) band gap of material goes on decreasing. In the Photocatalytic degradation at x= 0.3 got highest degradation ~ 73%. As the band gap goes on decreasing enhancing the photocatalytic performance.

Acknowledgment

The authors are thankful to the Dr. D. H. Bobade for his valuable suggestions to strengthen the manuscript and also thankful to Dr. Babaji Ghule and Mr. Anil Kawade for their technical support. And also support to Chandmal Tarachand Bora Arts Commerce and science college Shirur for help in X-RD Characterization. And also support to Department of physics B.P.H.E. Society's Ahmednagar College Ahmednagar Savitribai Phule Pune University Pune.

Financial support and sponsorship

Nil.

Conflicts of interest

The authors declare that there are no conflicts of interest regarding the publication of this paper.

References:

1. Soler MA, Paterno LG. Magnetic nanomaterials. InNanostructures 2017 Jan 1 (pp. 147-186). William Andrew Publishing.
2. Han JK, Choi HJ. Non-stoichiometric zinc-doped spinel ferrite nanoparticles with enhanced magnetic property and their magnetorheology. Colloid and Polymer Science. 2018 Feb;296:405-9.
3. Tovstolytkin AI, Kulyk MM, Kalita VM, Ryabchenko SM, Zamorskyi VO, Fedorchuk OP, Solopan SO, Belous AG. Nickel-zinc spinel nanoferrites: Magnetic characterization and prospects of the use in self-controlled magnetic hyperthermia. Journal of Magnetism and Magnetic Materials. 2019 Mar 1;473:422-7.
4. Kefeni KK, Mamba BB. Photocatalytic application of spinel ferrite nanoparticles and nanocomposites in wastewater treatment. Sustainable materials and technologies. 2020 Apr 1;23:e00140
5. Reddy DH, Yun YS. Spinel ferrite magnetic adsorbents: alternative future materials for water purification?. Coordination Chemistry Reviews. 2016 May 15;315:90-111.
6. Sharma R, Thakur P, Kumar M, Thakur N, Negi NS, Sharma P, Sharma V. Improvement in magnetic behaviour of cobalt doped magnesium zinc nano-ferrites via co-precipitation route. Journal of alloys and compounds. 2016 Nov 5;684:569-81
7. Kotsikau D, Ivanovskaya M, Pankov V, Fedotova Y. Structure and magnetic properties of manganese–zinc-ferrites prepared by spray pyrolysis method. Solid State Sciences. 2015 Jan 1;39:69-73.
8. Mathew DS, Juang RS. An overview of the structure and magnetism of spinel ferrite nanoparticles and their synthesis in microemulsions. Chemical engineering journal. 2007 May 1;129(1-3):51-65.
9. Petrova E, Kotsikau D, Pankov V. Structural characterization and magnetic properties of sol–gel derived ZnxFe3–xO4 nanoparticles. Journal of Magnetism and Magnetic Materials. 2015 Mar 15;378:429-35.
10. Chen L, Shen Y, Bai J. Large-scale synthesis of uniform spinel ferrite nanoparticles from hydrothermal decomposition of trinuclear heterometallic oxo-centered acetate clusters. Materials Letters. 2009 May 15;63(12):1099-101.
11. Ghasemi A, Ashrafizadeh A, Paesano Jr A, Machado CF, Shirsath SE, Liu X, Morisako A. The role of copper ions on the structural and magnetic characteristics of MgZn ferrite nanoparticles and thin films. Journal of magnetism and magnetic materials. 2010 Oct 1;322(20):3064-71.
12. dimitrov d, kolentsova e, dospatliev l, ivanova m. comparison of the catalytic activity of cu-mn supported catalysts prepared by standard impregnation method and solution combustion synthesis. oxidation communications. 2020 jul 1;43(3).
13. Verma A, Thakur OP, Prakash C, Goel TC, Mendiratta RG. Temperature dependence of electrical properties of nickel–zinc ferrites processed by the citrate precursor technique. Materials Science and Engineering: B. 2005 Jan 15;116(1):1-6.
14. Tatarchuk TR, Bououdina M, Paliychuk ND, Yaremiy IP, Moklyak VV. Structural characterization and antistructure modeling of cobalt-substituted zinc ferrites. Journal of Alloys
15. Hou WX, Wang Z. Structural and magnetic properties of Ni0. 15Mg0. 1Cu0. 3Zn0. 45Fe2O4 ferrite prepared by NaOH-precipitation method. Materials Science and Engineering: B. 2015 Sep 1;199:57-61.
16. Chen L, Shen Y, Bai J. Large-scale synthesis of uniform spinel ferrite nanoparticles from hydrothermal decomposition of trinuclear heterometallic oxo-centered acetate clusters. Materials Letters. 2009 May 15;63(12):1099-101.
17. Pawar RA, Patange SM, Tamboli QY, Ramanathan V, Shirsath SE. Spectroscopic, elastic and dielectric properties of Ho3+ substituted Co-Zn ferrites synthesized by sol-gel method. Ceramics International. 2016 Nov 1;42(14):16096-102.
18. Ashour AH, El-Batal AI, Maksoud MA, El-Sayyad GS, Labib SH, Abdeltwab E, El-Okr MM. Antimicrobial activity of metal-substituted cobalt ferrite nanoparticles synthesized by sol–gel
19. Gabal MA, Al-Juaid AA, El-Rashed S, Hussein MA. Synthesis and characterization of nano-sized CoFe2O4 via facile methods: A comparative study. Materials Research Bulletin. 2017 May 1;89:68-78.

20. Yadav RS, Havlica J, Hnatko M, Šajgalík P, Alexander C, Palou M, Bartoníčková E, Boháč M, Frajkorová F, Masilko J, Zmrzlý M. Magnetic properties of Co1− xZnxFe2O4 spinel ferrite nanoparticles synthesized by starch-assisted sol–gel autocombustion method and its ball milling. Journal of Magnetism and Magnetic Materials. 2015 Mar 15;378:190-9
21. Effect of aluminium doping on structural, optical, photocatalytic and antibacterial activity on nickel ferrite nanoparticles by sol–gel auto-combustion method Published: 09 October 2018 Volume 29, pages 20395–20414, (2018)
22. A. Manikandan, J.J. Vijaya, L.J. Kennedy, M. Bououdina, Structural, optical and magnetic properties of Zn1−xCuxFe2O4 nanoparticles prepared by microwave combustion method. J. Mol. Struct. 1035, 332 (2013)
23. R. Saranya, R.A. Raj, M.S. AlSalhi, S. Devanesan, Dependence of catalytic activity of nanocrystalline nickel ferrite on its structural, morphological, optical, and magnetic properties in aerobic oxidation of benzyl alcohol. J. Supercond. Nov. Magn. 31(4), 1219 (2018)
24. J.El Ghoul, Synthesis, structural and optical properties of nanoparticles (Al, V) co-doped zinc oxide. Bull. Mater. Sci. 39, 7 (2016).
25. Visible-Light-Induced Photocatalyst Based on Cobalt-Doped Zinc Ferrite Nanocrystals Guoli Fan† Ji Tong† Feng Li*† Industrial & Engineering Chemistry Research Vol 51/Issue 42
26. M.I. Khan, Zahra Saman, Ali Mujtaba, M.S. Hasan, Ming Zhang, Safa Ezzine. Tailoring the structural, morphological, optical, photocatalysis, and electrical characteristics of Zn0.5Mg0.5-xCoxLa0.1Fe1.9O4 ferrites across cobalt concentration from x = 0.0–0.2. Materials Science and Engineering: B **2025**, *319* , 118352
27. Kalyani K. Deshmukh, Shital.P. Nawale, Kajal A. Gurav, Swapnil Bhagat, Atul P. Keche, K.M. Jadhav. Impact of Mn2+- Ti4+ dopant on the photocatalytic dye degradation efficiency of cobalt ferrite nanoparticle. Ceramics International **2025**, *49*
28. Md. Dipu Malitha, Md. Tamzid Hossain Molla, Md. Abul Bashar, Dipesh Chandra, Md. Shameem Ahsan. Fabrication of a reusable carbon quantum dots (CQDs) modified nanocomposite with enhanced visible light photocatalytic activity. Scientific Reports **2024**, *14* (1)
29. Sankeetha Sasikumar, Arulmozhi Rajaram. The synergetic effect of cobalt-doped zinc ferrite and hexagonal boron nitride photocatalyst for wastewater treatment. Diamond and Related Materials **2024**, *147* , 111270.
30. Nanda Saridewi, Dienda Juita Utami, Agustino Zulys, Siti Nurbayti, Nurhasni, Adawiah, Anggina Rahma Putri, Rumi Kamal. Utilization of Lidah mertua (Sansevieria trifasciata) extract for green synthesis of ZnFe2O4 nanoparticle as visible-light responsive photocatalyst for dye degradation. Case Studies in Chemical and Environmental Engineering **2024**, *9* , 100745